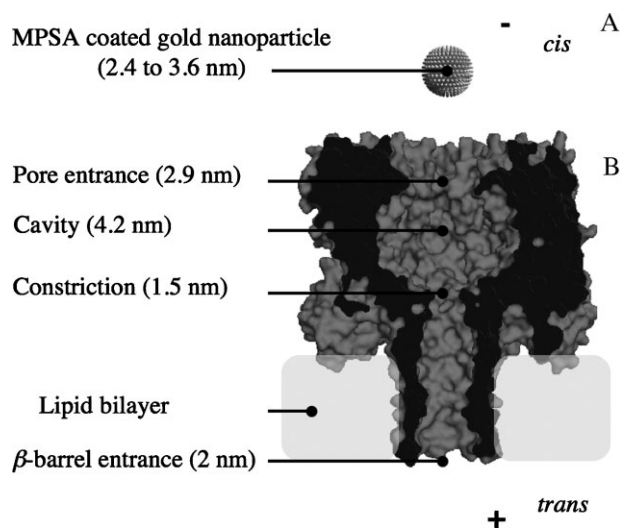


# Electrophysiological Study of Single Gold Nanoparticle/ $\alpha$ -Hemolysin Complex Formation: A Nanotool to Slow Down ssDNA Through the $\alpha$ -Hemolysin Nanopore\*\*

Yann Astier,<sup>\*</sup> Oktay Uzun, and Francesco Stellacci

$\alpha$ -Hemolysin ( $\alpha$ HL) is a heptameric protein pore (Figure 1) for which the X-ray structure is resolved.<sup>[1]</sup> The ability of  $\alpha$ HL to insert into an insulating lipid bilayer separating two chambers of aqueous electrolyte has made it a useful system to measure the ionic current that passes through the pore under an applied potential.<sup>[2,3]</sup> When an analyte interacts with a binding site within the pore, a significant change in the pore conductivity is observed. At fixed potential, the extent and duration of the current block from each binding event help reveal the identity of the analyte, while the frequency of the binding events reveals the analyte concentration. Chemical and biomolecular engineering of  $\alpha$ HL permit the stochastic sensing of molecules by tailoring internal analyte binding sites.<sup>[3]</sup> Since the pioneering work of Bezrukov and Kasianowicz on the discrimination between  $H^+/D^+$  ions, laying the physical basis for nanopore-based detection of analytes, detection, quantification, and characterization of ssRNA and ssDNA were described and led to “nanopore force spectroscopy” using  $\alpha$ HL.<sup>[4–8]</sup> Single-base mismatch in a short polynucleotide strand, toxic metal ions, drugs, enantiomers, TNT, and nucleotides have also been specifically detected.<sup>[2,9–13]</sup> Covalent attachment of different compounds within the pore have also been reported for the study of cis-trans isomerization of azobenzene, the multistep formation or breaking of covalent bonds, and the hybridization of DNA oligonucleotides.<sup>[14–20]</sup> Poly(ethylene glycol) (PEG) and whole PAMAM dendrimers have also been reported to enter and covalently attach inside  $\alpha$ HL.<sup>[21–23]</sup> Metal nanoparticles

are supramolecular assemblies of a self-assembled monolayer (SAM) onto an inorganic nanocrystal.<sup>[24,25]</sup> They offer unique opportunities for interfacing nanopore technologies with molecular and macromolecular sensing as they combine the properties of the inorganic core as single-electron charging, magnetism and rigidity, with those of the ligand shell for solubility, pseudo-enzymatic behavior, and multivalency.<sup>[26–31]</sup> To the best of our knowledge, for the first time we describe how it is possible to trap single-monolayer-protected gold nanoparticles in the  $\alpha$ -hemolysin ( $\alpha$ HL) nanopore, and study its size, charge, and surface properties. We show the unique conductance signature of a single sodium 3-mercaptopropylsulfonate (MPSA)-coated gold nanocrystal trapped inside the  $\alpha$ HL “cap” at constant potential, and its ionic current correction at ramping potential. We report how the transmembrane potential amplitude conditions the size of the nanoparticle being trapped inside the pore, as well as the correlation between the size of the trapped nanoparticle and its dwell time ( $\tau_{off}$ ). We find that the largest nanoparticle observed to enter the pore yields a 50% block of the pore conductance. The space between the nanoparticle and the inner-pore surface can be as small as 0.8 nm (considering the



**Figure 1.** A) Cartoon of a MPSA monolayer protected nanoparticle. B) Inner structure of the heptameric  $\alpha$ HL pore. The model was obtained by clipping the whole protein structure from its published pdb file [1] in MacPyMol. By convention, the ground electrode is located in the *trans* compartment, and the transmembrane potential sign is applied to the electrode in the *cis* compartment.

[\*] Dr. Y. Astier

Instituto de Quimica e Tecnologia Biologica  
Universidade Nova de Lisboa  
Av. Da Republica, EAN, 2784-505, Oeiras (Portugal)  
E-mail: yannastier@itqb.unl.pt

Dr. O. Uzun, Prof. F. Stellacci  
Department of Materials Science and Engineering  
Massachusetts Institute of Technology  
77 Massachusetts Avenue, Cambridge, MA 02139 (USA)

[\*\*] The authors thank Prof. Hagan Bayley and Qihong Li for providing the purified *S. aureus*  $\alpha$ -hemolysin monomer, Dr. Nunes for assistance with statistics analysis, the ITQB, and the MIT Portugal program for financial support. We acknowledge support of the Singapore MIT Alliance 2 and NSF CAREER award. F.S. is grateful for the generous support of the Packard Foundation.

Supporting Information is available on the WWW under <http://www.small-journal.com> or from the author.

DOI: 10.1002/sml.200801779

largest nanoparticle capable of entering the pore entrance of 2.9 nm). We report the ability of the nanoparticle/nanopore complex to allow other molecules to enter the pore. Single-stranded DNA (ssDNA) was seen to thread through the nanoparticle/nanopore complex. Our results show that the complex permeability to ssDNA depends on the chemical nature of the nanoparticle coating and the transmembrane potential applied. This system offers a novel nanotool aimed at controlling the threading speed of ssDNA through  $\alpha$ HL. These results open a new field where nanoparticle surface properties are confined to the tight cavity formed by the inside of the  $\alpha$ HL nanopore cap.

Gold nanoparticles ( $\approx 2$ -nm metal core diameter) coated with 3-mercaptopropylsulfonic acid (MPSA) as well as mixtures of MPSA/octanethiol (OT) organic ligands were synthesized using a previously published approach.<sup>[32]</sup> They were extensively purified from free ligands using filtration so that their  $^1\text{H}$  NMR spectra were composed only of broad peaks. The size distribution of the nanoparticle metallic core was assessed by TEM (Supporting Information, Table S1 and Figure S1). The average core size of the gold nanoparticles was found to be 1.9 nm (std dev 0.6 nm,  $n = 290$ ). The overall size of the nanoparticles ( $3.0 \pm 0.6$  nm) was calculated by adding the metal core radii measured from TEM images and two times the extended MPSA ligand length (1.1 nm) estimated using Chem 3D Pro. We found that particles with a sufficiently small diameter ( $< 2.9$  nm) could individually enter an  $\alpha$ HL nanopore cavity when a potential is applied to drive the negatively charged nanoparticles into the pore.

Figure 2A shows a typical single-pore ionic current when the potential is ramped from 0 to 200 mV in 5 s and decreased back to 0 V at the same scan rate. When the pore is empty, the ionic current increases (and decreases) roughly linearly with voltage (Figure 2A). In the presence of gold nanoparticles on the *cis* side a drop in current (E1) is observed when the potential is increased, the resulting ionic current has a lower intensity than that of the empty pore, and the shape of the  $I$ - $V$  curve reveals a negative correction of the current (Figure 2B). As the potential decreases, a rise in current (at the potential

E2) is observed. The final part of the sweep is identical to the empty pore control. The distribution of E1 and E2 over 298 scans ( $n = 5$ ) is plotted in columns on the time axis of Figure 2B. The distributions of E1 and E2 reveal that E1 systematically occurs at a higher potential than E2. We suggest that E1 is due to the entry of a nanoparticle into the pore, and E2 is generated by its exit once the potential is no longer sufficient to hold the negatively charged nanoparticle inside the  $\alpha$ HL cavity. This interpretation is supported by control experiments with just the nanoparticle ligands as well as with other starting materials for the nanoparticle synthesis showing no influence on the current-time plots (Supporting Information). While Figure 2B shows the recording of a single-nanoparticle capture and release, Figure S4 shows a similar scan where two E1 events are observed, followed by one E2 event occurring in the course of the potential scan. This reveals that more than one nanoparticle can be captured as the transmembrane potential is increased. This implies that two negatively charged nanoparticles are held in close proximity inside the pore, and surface charge shielding may be occurring. Figure S2 shows that when a large single nanoparticle is captured (i.e., conductance of the nanopore is reduced to 50%) no second E1 event is observed, and most importantly, the nanoparticle is not released from the pore at open circuit (Figure S2B). Figure S2B also reveals the strong negative correction of the  $I$ - $V$  curve generated by the trapped nanoparticle.

The conductance of the pore is a function of the available space between the nanoparticle surface and the inner pore. If we consider the inner pore to be a sphere of 4.5-nm diameter (radius  $r_p$ ), when a nanoparticle of radius  $r_{np}$  is trapped the free volume inside the pore cap is given by the inner pore cap volume less the volume occupied by the nanoparticle. The free volume  $V_f$  is therefore:

$$V_f = 4/3\pi(r_p^3 - r_{np}^3) \quad (1)$$

( $V_f, \text{m}^3$ ,  $r_p = 2.25 \cdot 10^{-9} \text{m}$ ,  $r_{np}, \text{m}$ ).  $V_f$  is a cubic function of the particle radius. However, we can't establish the exact correlation between the conductance and the free volume  $V_f$  because the electrostatic effect of the MPSA coating on the ionic current needs to be calculated. The full modeling will be published separately.

Figure 3A shows a constant potential recording of the capture of MPSA-coated nanoparticles at 80 mV. The nanoparticle/nanopore complex appears to have current intensity sublevels (Figure 3A). Event 1 displays two sublevels with  $\approx 3$  pA amplitude difference and the histogram of event 2 reveals five such sub-levels spread over  $\approx 10$  pA. The possibility that these sublevels are the result of stochastic molecular interactions with the nanoparticle surface from trace contaminations in the solution can not be ruled out but given their high frequency of occurrence, their defined amplitudes, and their persistence across experiments with different batches of nanoparticles and different buffer solutions, they are more probably due to movements or "fluctuations" of the nanoparticle inside the nanopore. The amplitude sublevels are still observed when a square wave AC voltage (4 mV

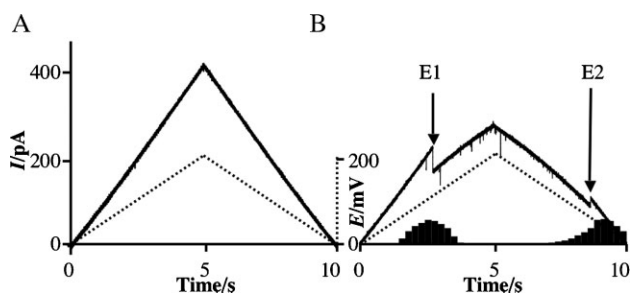


**Figure 2.** A) Ionic current recording of a single  $\alpha$ HL pore (black). The cyclic potential waveform between 0 and 200 mV at  $40 \text{ mVs}^{-1}$  (dotted). The experiment is carried out at pH 8.1 Tris-HCl 0.1M, 2M KCl. B) Ionic current recording (black) of a single pore with  $1.9 \mu\text{M}$  MPSA-coated gold nanoparticles (3.02-nm diameter) in the *cis* compartment of the cell. A drop in current intensity is labeled E1 while voltage (dotted) is increasing, and a rise in current intensity labeled E2 is observed while voltage is decreased. On the time axis a distribution of the E1 and E2 events is plotted into columns for 298 values ( $n = 5$ ).

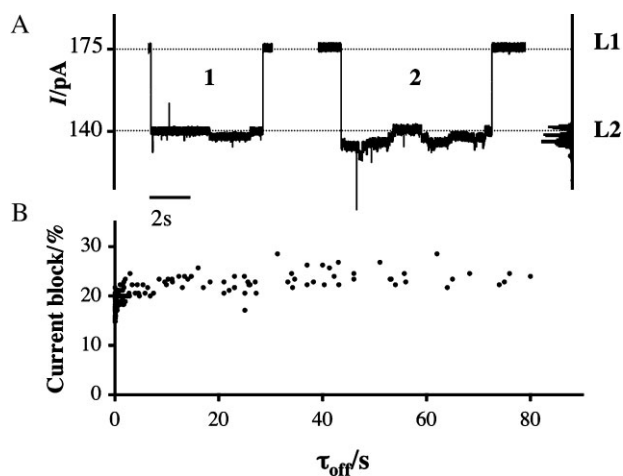


**Figure 3.** A) The current recording of a single  $\alpha$ HL pore in 2M KCl, pH 8.1 Tris-HCl buffer 0.1M at 80 mV. The empty pore current **L1** is 175 pA, and stochastically drops to approximately 140 pA (**L2**) in the presence of 4.4  $\mu\text{M}$  MPSA gold nanoparticles. Two capture events are represented revealing changes of current intensity between defined amplitude levels, while the nanoparticle is inside the pore. A histogram of the amplitude changes of event 2 is plotted on the right. B) Correlation between  $\tau_{\text{off}}$  and the current block of a pore by a given nanoparticle at 80mV in the conditions described above (198 points,  $n = 4$ ).

amplitude, frequency from 1 to 6 KHz) is superimposed to a constant 100mV potential (not shown). The pore entry diameter is smaller than the pore cavity diameter (Figure 1); for any nanoparticle that fits through the pore entry, space is available around the nanoparticle for movement.

Figure 3B shows the dwell time ( $\tau_{\text{off}}$ ) increasing with the current block at constant potential. Current block values below 15%, were not observed; this current block value may correspond to the size of the smaller nanoparticles present in the solution.

The decrease of the open pore time  $\tau_{\text{on}}$  with the increase of the transmembrane potential (Table 1), shows that the nanoparticle capture is electrically driven. The net negative charge of each nanoparticle is a function of the number of MPSA ligands at its surface, therefore larger nanoparticles will carry more charges. The average current block (i.e., particle size) of the captured nanoparticle increases with voltage. The pore entrance diameter (2.9 nm, Figure 1) restricts the size of the nanoparticle entering the pore; as the diameter of the particles increases towards the diameter of the pore entry, the probability to enter is lower unless the transmembrane

potential is increased. The dwell time ( $\tau_{\text{off}}$ ) of the nanoparticles inside the pore becomes semi-infinite above 140 mV. The voltage ramping experiments (Figure 2B) show that the average  $E1$  value for these nanoparticles is 98 mV (std dev = 18 mV).

The current block induced by the trapped nanoparticles was found to vary between 15 and 50% (Figure S3). We observed that nanoparticles inducing the largest current block have a lower  $E2$  potential. These experiments were carried out at low nanoparticle concentration (24 nM) to avoid multiple particle capture, and only single nanoparticle events were logged. The transmembrane potential is used to oppose a “fluctuation force” driving the nanoparticle out of the pore. When the potential decreases to the point where the electric force is equal to the “fluctuation force”, the particle is released. Figure S3 reveals a correlation between the size of the particle and the  $E2$  potential. The freedom of movement or “fluctuation” of a captured nanoparticle depends on the free space available inside the pore, which we interpret as an inverted correlation between the particle size and the “fluctuation force” intensity. Furthermore, we see from Figure S4 that when two relatively small nanoparticles are captured, the release potential  $E2$  is lower than what is observed in Figure S3 where strictly single particle captures are reported.

We compared the entry and exit potentials of a series of particles coated with a mixture of ligands (Table S2). The particles were coated with different ratios of MPSA and OT. OT is longer than MPSA when fully extended hence even though these particles were of similar core size to the all MPSA ones, their total size was larger. All the mixed ligand particles had extremely similar size (same average core size of 2.1 nm), allowing comparison among them. The composition of the ligand shell is assumed to be the one used in the synthesis reaction. Our previous studies suggest that these particles have a structured ligand shell, where phase separation among the ligands occurs.<sup>[28,32–35]</sup> However, we have not yet established if these particles display the ordered striations observed on other systems.<sup>[36,37]</sup> Table S2 shows how  $E1$  varies from all MPSA coated nanoparticles to MPSA:OT (2:1), and MPSA: (1:2).  $E1$  shows a variation with ligand shell composition that is non-monotonic. In fact the highest voltage required to force entrance of the nanoparticles is for the 1:1 composition. This result would seem to suggest an important role of the ligand shell in mediating the entrance. The non-monotonic behavior is in line with the solubility of particles

**Table 1.** Summary of the MPSA nanoparticle capture events in a single  $\alpha$ HL pore in 2M KCl, pH 8.1 Tris-HCl buffer 0.1 M at voltages ranging from 60 to 200 mV. Each value is the average of  $p$  measurements, and is given  $\pm$  the standard deviation.

$E$ [mV]	$\tau_{\text{on}}[s]$ ( $\pm$ std dev)	$\tau_{\text{off}}[s]$ ( $\pm$ std dev)	Current block[%] ( $\pm$ std dev)	$p$
60	218 $\pm$ 105	<1	18.5 $\pm$ 2.5	153
80	33 $\pm$ 53.6	14 $\pm$ 20.6	21 $\pm$ 6	198
100	9.22 $\pm$ 9.4	53 $\pm$ 46	23 $\pm$ 11	160
120	3.24 $\pm$ 2.2	80 $\pm$ 63	26.5 $\pm$ 12.3	157
140	1.21 $\pm$ 1.4	>100	30 $\pm$ 9.7	133
160	0.33 $\pm$ 0.4	>100	34 $\pm$ 10	88
180	0.28 $\pm$ 0.4	>100	37 $\pm$ 10.7	103
200	0.21 $\pm$ 0.4	>100	43.8 $\pm$ 12.5	98

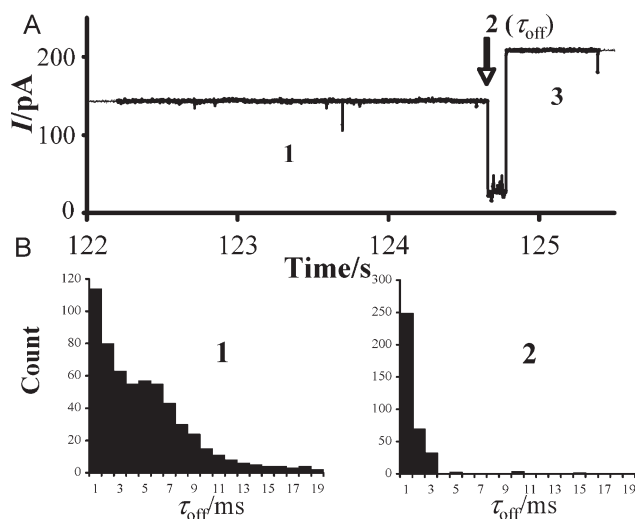


**Figure 4.** A shows the current recording of a single  $\alpha$ HL pore in 2 M KCl, pH 8.1 Tris-HCl buffer 0.1 M at 100 mV, 100 nm 60mer ssDNA 5'(A<sub>5</sub>C<sub>5</sub>)<sub>6</sub>3', 4.4  $\mu$ M nanoparticle in the cis chamber. **1** is the recording of the pore with a single nanoparticle trapped inside. **2** is a 150 ms blocking event (94% current block). **3** is the empty pore current amplitude of 215 pA. **B** shows the distribution of toff values **1** when a nanoparticle is previously captured in the pore, **2** when no nanoparticle is present in the pore.

with structured ligand shells observed in previous works, highlighting the important role of the solvent around the particles.

The permeability of the nanoparticle/nanopore complex towards ssDNA revealed marked differences in behaviour between gold nanoparticles coated with different ratios of MPSA to OT ligand. Figure 4A shows that when a MPSA nanoparticle is trapped inside the pore, and ssDNA is present in the solution, every nanoparticle trapping event (**1**) is terminated by a 93–98% current block (**2**), which is immediately followed by a return to the empty pore current intensity (**3**). The same pattern is observed for any potential from 100 to 200 mV (not shown), whether the DNA is added before or after the nanoparticle is trapped in the pore. The ssDNA sequence was chosen to rule out any secondary structure. The 94% current block observed in Figure 4 is consistent with ssDNA threading through the  $\beta$ -barrel of  $\alpha$ HL, and the return to empty pore current suggests that the ssDNA threading through the pore results in the expulsion of the nanoparticle.<sup>[5]</sup> We find the larger nanoparticles remain in the pore for several more minutes than the others, but end in the same sequence of events as the smaller ones. From these results, it is not clear if the ssDNA threading initiates while the nanoparticle is still trapped inside the cap, or if it is released

simultaneously with the entrance of ssDNA. The ability of two negatively charged nanoparticles to reside next to each other inside the pore cavity suggests that the negatively charged ssDNA and the nanoparticle may be able to do the same. Figure 4B shows the distribution of  $\tau_{\text{off}}$  from event (**2**). It demonstrates that in the presence of a nanoparticle trapped inside the pore significantly increases the  $\tau_{\text{off}}$  of event (**2**). Table 2 compares the  $\tau_{\text{off}}$  values between a 60mer ssDNA (587 values) and an 80mer ssDNA (801 values). The  $\tau_{\text{off}}$  distributions of both ssDNA were fitted with multiple Gaussian peaks (Figure S5) and the 60mer average  $\tau_{\text{off}}$  value was found to be 5 ms whereas the toff in the absence of nanoparticle is 0.4 ms. The 80mer displays two different peaks at 4. and 8. ms (as opposed to 0.56 ms in the absence of nanoparticle) that could be reflecting the 3' or 5' orientation of the ssDNA as it threads past the nanopore/nanoparticle complex. When OT is present at the surface of the nanoparticle (particle size being equal, Table S1), the entry and exit potential inside the pore are seen to remain identical to those of all MPSA particles (Table S2). However, we observe a marked difference in behaviour towards ssDNA interaction inside the pore (Table 2) where the presence of hydrophobic ligand OT generates a high resistance to ssDNA entering the nanoparticle/nanopore complex. Each type of nanoparticle was checked for size and  $E1$  and  $E2$  potential (supplementary material) to insure comparability of the results. We observed, that MPSA nanoparticles allow ssDNA to thread from 100 mV, while MPSA2:OT1 and MPSA1:OT2 require a transmembrane potential of 200 mV. This result illustrates how the nanoparticle surface coating properties can influence the permeability of the nanoparticle/nanopore complex towards large molecules such as ssDNA.

In conclusion, we have shown that individual gold nanoparticles can be trapped inside the  $\alpha$ HL pore while retaining at least 50% of the nanopore conductance. The nanoparticle surface functionalization confers ionic and molecular selectivity to the nanopore it is trapped into. The nanoparticle trapping is a voltage dependent process, and the size of the nanoparticles thus trapped is defined by the voltage intensity. We tested ssDNA threading, and observed that nanopore/nanoparticle complex is a promising nanotool to control the threading speed of ssDNA through the  $\alpha$ HL nanopore. The inorganic crystal surface properties can be further adjusted using different ligand types and combinations to help improve the interaction with ssDNA. In future experiments, we hope to use genetic engineering of the nanopore inner structure in combination with the nanoparticle surface properties to tailor specific physico-chemical environments to improve the control over the threading speed of ssDNA through the  $\alpha$ HL nanopore.

**Table 2.**  $\tau_{\text{off}}$  values for the ssDNA 60mer and 80mer in the presence and the absence of nanoparticle. Values are obtained by fitting the  $\tau_{\text{off}}$  population with Gaussian distributions as described in Figure S5.

SsDNA length	60mer		80mer	
$n$	No Nanoparticle $n = 343$	Nanoparticle $n = 587$	No Nanoparticle $n = 453$	Nanoparticle $n = 801$
$\tau_{\text{off}1}$ [ms] ( $\pm$ std dev)	$0.406 \pm 0.03$ $R^2 = 0.99$	<1	$0.56 \pm 0.2$ $R^2 = 0.99$	<1
$\tau_{\text{off}2}$ [ms] ( $\pm$ std dev)	N/A	$4.48 \pm 0.44$ $R^2 = 0.99$	N/A	$3.53 \pm 0.7$ $R^2 = 0.99$
$\tau_{\text{off}3}$ [ms] ( $\pm$ std dev)	N/A	N/A	N/A	$13.39 \pm 2.6$ $R^2 = 0.99$



- [21] S. Howorka, L. Movileanu, X. Lu, M. Magnon, S. Cheley, O. Braha, H. Bayley, *J. Am. Chem. Soc.* **2000**, *122*, 2411.
- [22] L. Movileanu, S. Howorka, O. Braha, H. Bayley, *Nat. Biotechnol.* **2000**, *18*, 1091.
- [23] H. Martin, H. Kinns, N. Mitchell, Y. Astier, R. Madathil, S. Howorka, *J. Am. Chem. Soc.* **2007**, *129*, 9640.
- [24] M. C. Daniel, D. Astruc, *Chem. Rev.* **2004**, *104*, 293.
- [25] A. C. Templeton, M. P. Wueling, R. W. Murray, *Accounts Chem. Res.* **2000**, *33*, 27.
- [26] S. W. Chen, R. S. Ingram, M. J. Hostetler, J. J. Pietron, R. W. Murray, T. G. Schaaff, J. T. Khoury, M. M. Alvarez, R. L. Whetten, *Science* **1998**, *280*, 2098.
- [27] A. K. Boal, B. L. Framkamp, O. Uzun, M. T. Tuominen, V. M. Rotello, *Chem. Mat.* **2004**, *16*, 3252.
- [28] A. M. Jackson, P. Jacob Silva, Y. Hu, F. Stellacci, *J. Am. Chem. Soc.* **2006**, *128*, 11135.
- [29] F. Stellacci, C. A. Bauer, T. Meyer-Friedrichsen, W. Wenseleers, V. Alain, S. M. Kuebler, S. J. K. Pond, Y. D. Zhang, S. R. Marder, J. W. Perry, *Adv. Mater.* **2002**, *14*, 194.
- [30] P. Pengo, S. Polizzi, L. Pasquato, P. Scrimin, *J. Am. Chem. Soc.* **2005**, *127*, 1616.
- [31] A. K. Boal, V. M. Rotello, *J. Am. Chem. Soc.* **2000**, *122*, 734.
- [32] O. Uzun, Y. Hu, A. Verma, S. Chen, A. Centrone, F. Stellacci, *Chem. Commun.* **2008**, 196.
- [33] G. A. De Vries, M. Brunnbauer, Y. Hu, A. M. Jackson, B. Long, B. T. Neltner, O. Uzun, B. H. F. Wunsch, F. Stellacci, *Science* **2007**, *315*, 358.
- [34] A. M. Jackson, J. W. Myerson, F. Stellacci, *Nat. Mater.* **2004**, *3*, 330.
- [35] A. Centrone, Y. Hu, A. M. Jackson, G. Zerbi, F. Stellacci, *Small* **2007**, *3*, 814.
- [36] R. P. Carney, G. A. De Vries, C. Dubois, H. Kim, J. Y. Kim, C. Singh, P. K. Ghorai, J. B. Tracy, R. L. Stiles, R. W. Murray, S. C. Glotzer, F. Stellacci, *J. Am. Chem. Soc.* **2008**, *130*, 798.
- [37] C. Singh, P. K. Ghorai, M. A. Horsch, A. M. Jackson, R. G. Larson, F. Stellacci, S. C. Glotzer, *Phys. Rev. Lett* **2007**, *99*.

Received: November 28, 2008

Published online: February 25, 2009